Supplementary information

Large-area, High-resolution, Flexible X-Ray Scintillator Film Based on a Novel 0D Hybrid Cuprous Halide

Dandan Li[1], Linghang Kong[2,3], Liping Feng[2], Jie Su[1], Xing Guo[1], Hui Peng[3], Xue Zhao[1,4], Hanyuan Ding[1], Xueyan Chen[1], Fei Zhang[5], Linyuan Lian[5], Zhifeng Shi[5], Pengfei Fu[6], Zhenhua Lin[1], Jingjing Chang[1]**

[1]School of Microelectronics, Xidian University, Xi'an 710071, China.

[2]State Key Laboratory of Solidification Processing, School of Materials Science and Engineering, Northwestern Polytechnical University Xi'an 710072, China.

[3]State Key Laboratory of Featured Metal Materials and Life-Cycle Safety for Composite Structures, MOE Key Laboratory of New Processing Technology for Nonferrous Metals and Materials, and School of Resources, Environment and Materials, Guangxi University, Nanning 530004, China.

[4]Wuhan National Laboratory for Optoelectronics, Huazhong University of Science and Technology, Wuhan 430074, China.

[5]Key Laboratory of Materials Physics of Ministry of Education, School of Physics, Zhengzhou University, Zhengzhou 450052, China

[6]Shenzhen Institute of Advanced Technology, Chinese Academy of Sciences 518055, China

*zhaoxue@xidian.edu.cn

*jjingchang@xidian.edu.cn

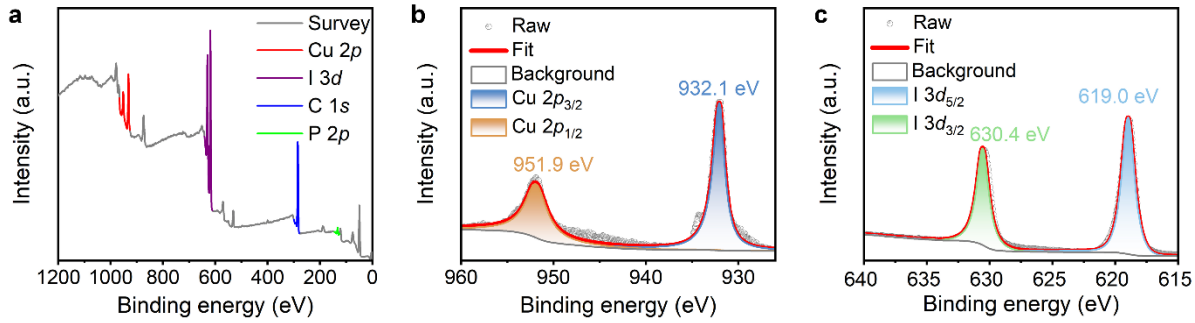

Fig. S1 X-ray photoelectron spectroscopy (XPS) spectra of $(MTP)_2Cu_4I_6$. **a** $(MTP)_2Cu_4I_6$ survey, **b** Cu 2*p*, and **c** I 3*d*.

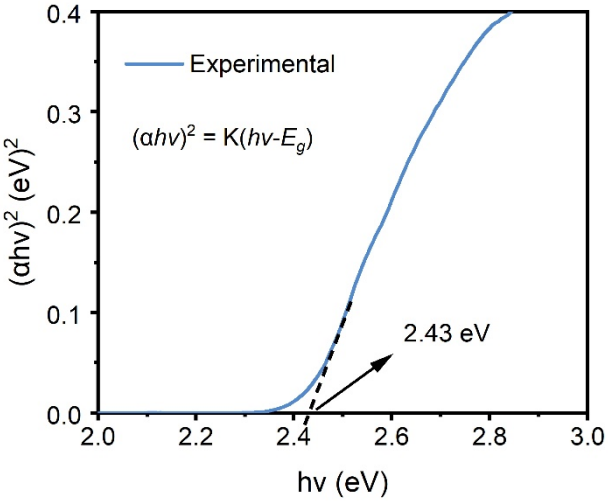

Fig. S2 $(MTP)_2Cu_4I_6$ bandgap derived from the *Tauc* plot.

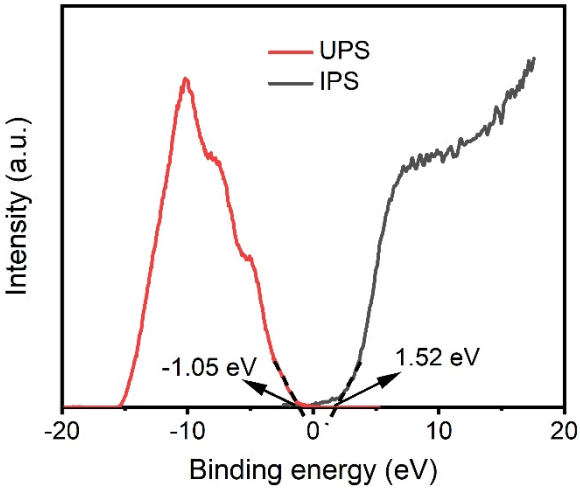

Fig. S3 Ultraviolet photoelectron spectroscopy and inverse photoelectron spectroscopy spectra of the $(MTP)_2Cu_4I_6$.

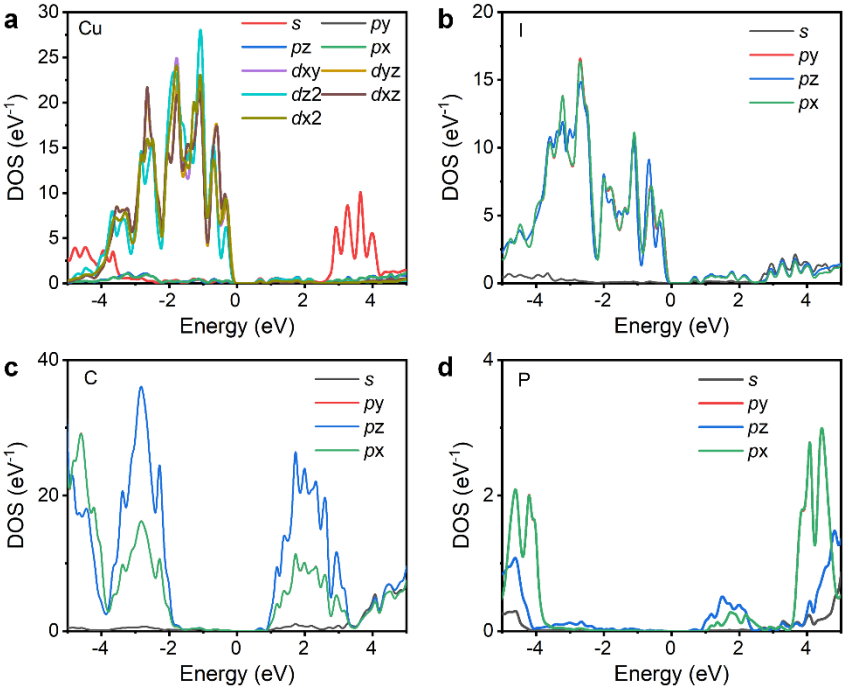

Fig. S4 Density of states of **a** Cu, **b** I, **c** C, and **d** P elements with energies from -5 to 5 eV.

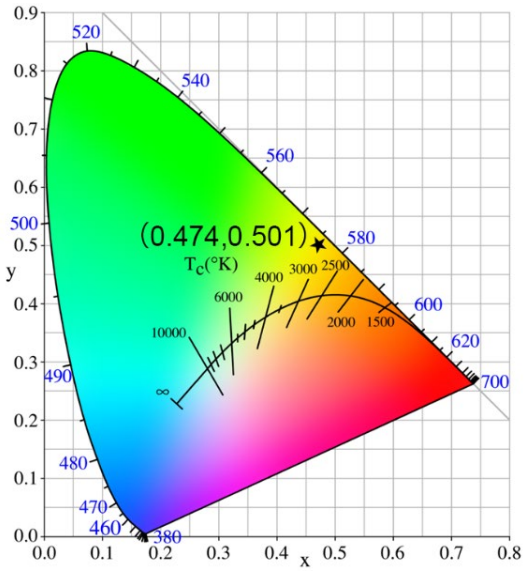

Fig. S5 Commission Internationale de l'Eclairage (CIE) chromaticity coordinates (black star) of emissions measured for $(MTP)_2Cu_4I_6$ samples in the CIE1931.

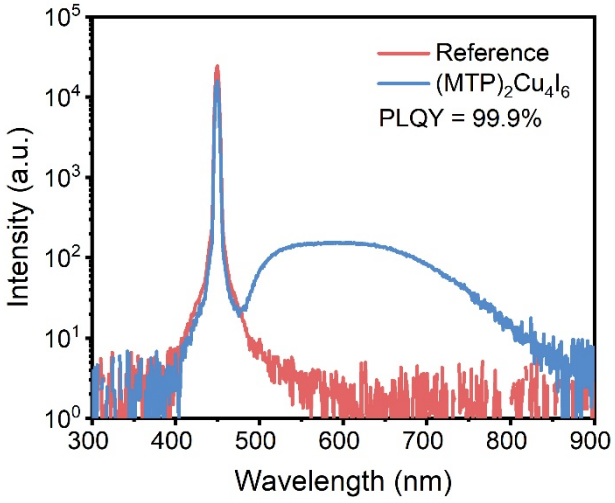

Fig. S6 Photoluminescence quantum yield (PLQY) curve of $(MTP)_2Cu_4I_6$ crystals. The reference curve is measured by placing a blank quartz plate in the integrating sphere.

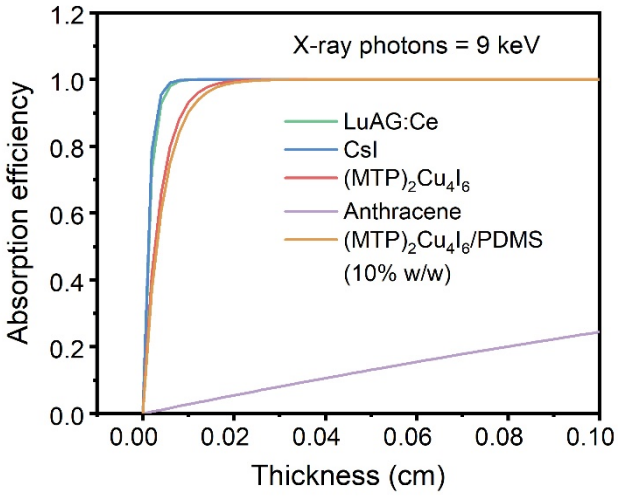

Fig. S7 Absorption efficiency of $(MTP)_2Cu_4I_6$, $(MTP)_2Cu_4I_6$/PDMS (10% w/w), CsI, LuAG:Ce, and anthracene as a function of thickness.

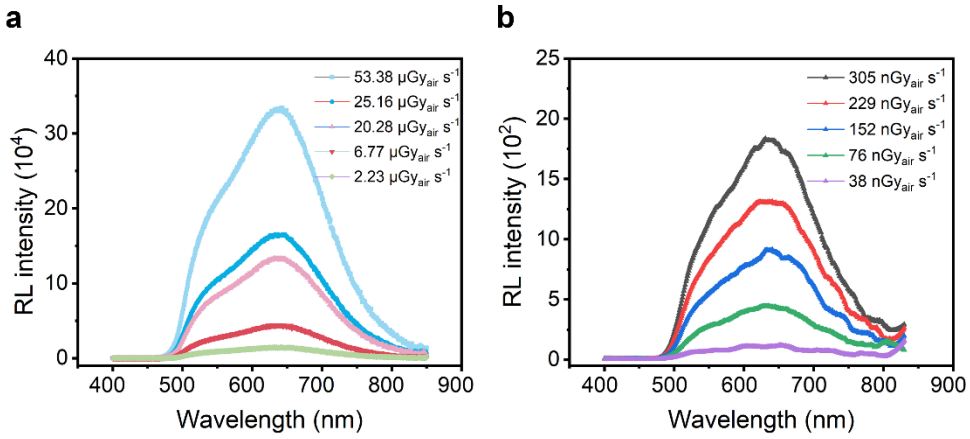

Fig. S8 Radioluminescence spectra of $(MTP)_2Cu_4I_6$ single crystals under **a** high, and **b** low-dose rate conditions.

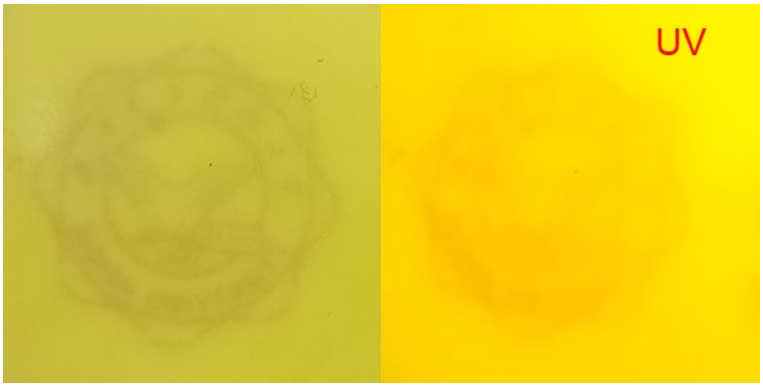

Fig. S9 Photographs of $(MTP)_2Cu_4I_6$/polydimethylsiloxane (PDMS) composite film under ambient light and 365 nm ultraviolet (UV) irradiation.

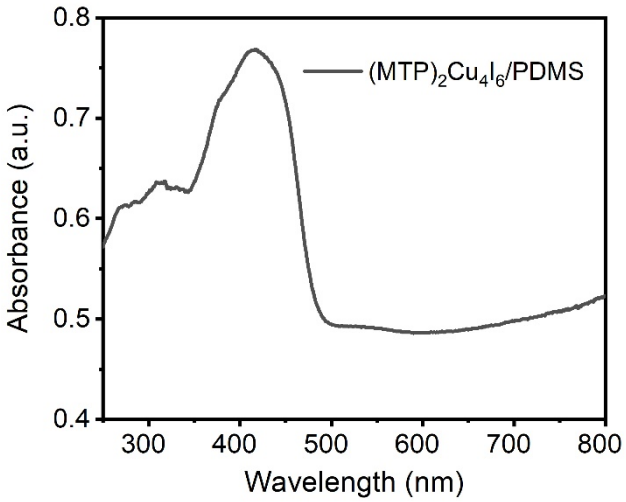

Fig. S10 UV-visible absorption spectrum of $(MTP)_2Cu_4I_6$/PDMS composite film.

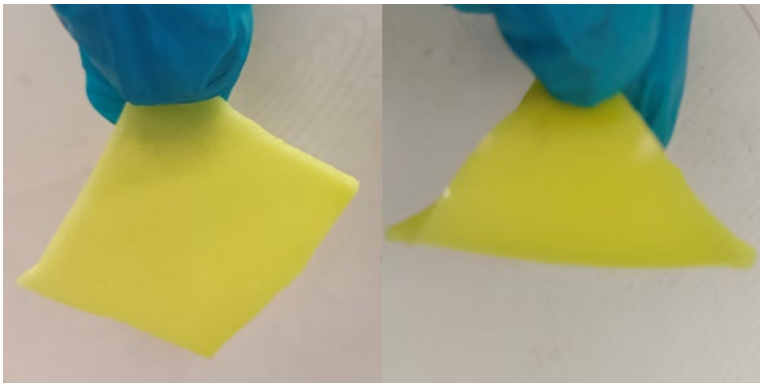

Fig. S11 Planar and nonplanar $(MTP)_2Cu_4I_6$/PDMS scintillator film images under ambient light conditions.

Fig. S12 Photograph of the standard tungsten edge.

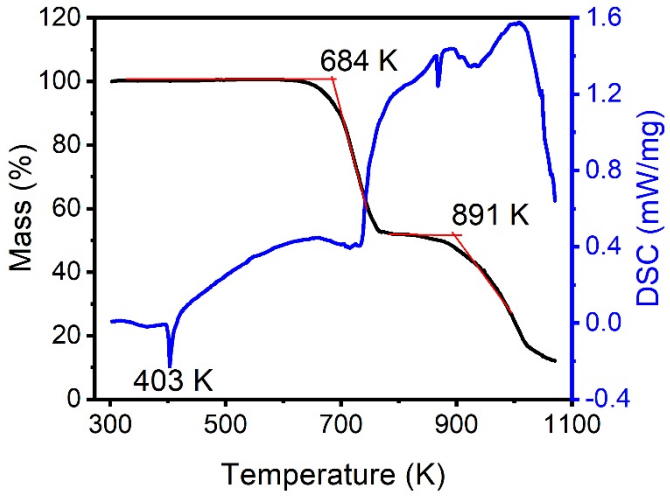

Fig. S13 Thermogravimetric analysis and differential scanning calorimetry curve of $(MTP)_2Cu_4I_6$ powder.

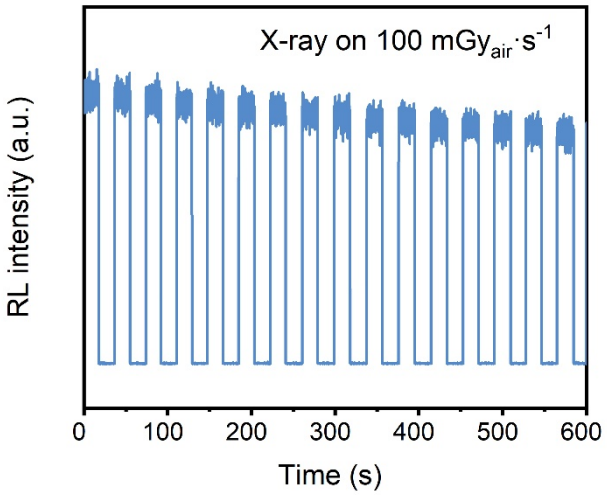

Figure S14 Emission photostability at 620 nm for the $(MTP)_2Cu_4I_6$/PDMS film following exposure to cyclical X-rays at a dose rate of 100 mGy_{air} s^{-1}.

Table S1. Crystal information from Checkcif of $(MTP)_2Cu_4I_6$ characterized by single-crystal X-ray diffraction.

Chemical formula	$(C_{19}H_{18}P)_2Cu_4I_6$
Temperature / K	193
Crystal system	Trigonal
Space group	*R*3*c*
a / Å	13.91190 (2)
b / Å	13.91190 (2)
c / Å	39.85970 (10)
α / °	90
β / °	90
γ / °	120
V / $Å^3$	6680.9392 (3)
M_r	1570.21
ρ_{calc} / (g cm^{-3})	2.342
μ / mm^{-1}	35.679
Z	6
F(000)	4368.0
Index ranges	-17<=*h*<=17, -17<=*k*<=17, -50<=*l*<=50

Table S2. Atomic ratios of C, P, Cu, and I in $(MTP)_2Cu_4I_6$ measured by XPS.

Elements	Atomic %
C	73.01
P	4.28
Cu	8.92
I	13.79
Total	100.00

Table S3. Comparison of PL properties and scintillation performance of reported cuprous halide scintillators.

Scintillator	PLQY (%)	Lifetime (μs)	Light yield (photons MeV^{-1})	Detection limit (nGy_{air} s^{-1})	Ref.
$(MTP)_2Cu_4I_6$	**99.9**	**2.18**	**43800**	**37.6**	**This work**
$[BzTPP]_2Cu_2I_4$	44.2	1.93	27700	352	1
$[BAPMA]Cu_2Br_5$	53.4	50.2	43700	74	2
$[ETPP]_2Cu_4Br_6$	94.2	32.89	53600	--	3
$[ETPP]CuBr_2$	65.2	2.75	58000	453	3
$C_9H_{20}NCuBrI$	99.5	2.52	25000	40.4	4
$(TBA)CuCl_2$	92.8	28.7	23400	--	5
$(TBA)CuBr_2$	80.5	232.05	24100	--	5
$(DIET)_3Cu_3Cl_3$	69.2	1.3	6000	--	6
$(DIET)_3Cu_3Br_3$	39.3	0.6	20700	189	6
$[Rb(18\text{-crown-}6)]_2Cu_4I_6$	93.4	2.4	10600	458.3	7
Rb_2CuCl_3	99.4	11.3	16600	88.5	8
K_2CuBr_3	87.0	64.3	23800	132.8	9
$Cs_3Cu_2I_5$	91.2	0.97	32000	--	10

BzTPP = Benzyltriphenylphosphonium; BAPMA = *N*,*N*-Bis(3-aminopropyl) methylamine; ETPP = Ethyltriphenylphosphonium; TBA = Tetrabutylammonium; DIET = 1,3-Diethyl-2-thiourea.

Table S4. Comparison of spatial resolution of reported cuprous halide scintillators.

Scintillator	Spatial resolution (lp mm^{-1})	Ref.
$(MTP)_2Cu_4I_6$/PDMS	**10.2**	**This work**
$[BzTPP]_2Cu_2I_4$/PVP	4.9	1
$[BAPMA]Cu_2Br_5$/PDMS	15.8	2
$C_9H_{20}NCuBrI$/PDMS	5.6	4
$(TBA)CuBr_2$/PVDF	3.0	5
$(DIET)_3Cu_3Br_3$/PDMS	11.7	6
$(C_8H_{20}N)_2Cu_2Br_4$ wafer	9.5	11
Rb_2CuBr_3/PS	1.7	12
$Cs_3Cu_2I_5$/PDMS	6.8	13

References

1. Lin, N. et al. 0D hybrid cuprous halide as an efficient light emitter and X-ray scintillator. *Laser & Photonics Reviews* **17,** 2300427 (2023).
2. Liu, Y. H. et al. Zero-dimensional hybrid cuprous halide of [BAPMA]Cu_2Br_5 as a highly efficient light emitter and an X-ray scintillator. *ACS Applied Materials & Interfaces* **15**, 20219-20227 (2023).
3. Li, D. Y. et al. Reversible triple-mode photo- and radioluminescence and nonlinear optical switching in highly efficient 0D hybrid cuprous halides. *Chemistry of Materials* **35**, 6598-6611 (2023).
4. Mao, P. et al. Organic-inorganic hybrid cuprous halide scintillators for flexible X-ray imaging. *ACS Applied Materials & Interfaces* **14**, 22295-22301 (2022).
5. Lian, L. Y. et al. Highly luminescent zero-dimensional organic copper halides for X-ray scintillation. *Journal of Physical Chemistry Letters* **12**, 6919-6926 (2021).
6. Han, K. et al. Promoting single channel photon emission in copper (I) halide clusters for X-ray detection. *Advanced Optical Materials* **10,** 2200865 (2022).
7. Almushaikeh, A. M. et al. Zero-dimensional Cu(I)-based organometallic halide with green cluster-centred emission for high resolution X-ray imaging screens. *Chemical Communications* **59**, 4447-4450 (2023).
8. Zhao, X. et al. All-inorganic copper halide as a stable and self-absorption-free X-ray scintillator. *Journal of Physical Chemistry Letters* **11**, 1873-1880 (2020).
9. Gao, W. R. et al. One-dimensional all-inorganic K_2CuBr_3 with violet emission as efficient X-ray scintillators. *ACS Applied Electronic Materials* **2**, 2242-2249 (2020).
10. Cheng, S. L. et al. Zero-dimensional $Cs_3Cu_2I_5$ perovskite single crystal as sensitive X-ray and γ-ray scintillator. *Physica Status Solidi-Rapid Research Letters* **14,** 2000374 (2020).
11. Su, B. B. et al. Ceramic wafer scintillation screen by utilizing near-unity blue-emitting lead-free metal halide $(C_8H_{20}N)_2Cu_2Br_4$. *Advanced Functional Materials* **33,** 2210735 (2023).

12. Han, L. L. et al. Environmentally stable one-dimensional copper halide based ultra-flexible composite film for low-cost X-ray imaging screens. *Chemical Engineering Journal* **430,** 132826 (2022).
13. Li, N. et al. Flexible, high scintillation yield $Cs_3Cu_2I_5$ film made of ball-milled powder for high spatial resolution X-ray imaging. *Advanced Optical Materials* **10,** 2102232 (2022).